Appendix 1 (article in press for IEEE Sensors Journal)

Manipulation of Microenvironment with a Built-in Electrochemical Actuator in Proximity of a Dissolved Oxygen Microsensor

Chang-Soo Kim*, Chae-Hyang Lee, Jason O. Fiering, Stefan Ufer, Charles W. Scarantino, and H. Troy Nagle

Chang-Soo Kim, Chae-Hyang Lee: Department of Electrical and Computer Engineering and Biological sciences, University of Missouri-Rolla, Rolla, MO 65409, USA. 573-341-4529 (voice), 573-341-4532 (fax), ckim@umr.edu, leecha@umr.edu

Jason O. Fiering: Draper Laboratory, 555 Technology Square, MS 37, Cambridge MA 02139, USA. 617-258-1596, jfiering@draper.com

Stefan Ufer, H. Troy Nagle: Biomedical MicroSensors Laboratory, Department of Electrical and Computer Engineering, North Carolina State University, Raleigh, NC 27695-7911, USA., 919-515-3578 (voice), 919-513-3814 (fax), t.nagle@ncsu.edu; stufer@eos.ncsu.edu

Charles W. Scarantino: Sicel Technologies, Inc., 3800 Gateway Center Blvd. Suite 308, Morrisville, NC 27560, USA. 919-465-2236 (voice), 919-465-0153 (fax), cw.scarantino@rexhealth.com

* Corresponding author

Abstract – Biochemical sensors for continuous monitoring require dependable periodic self-diagnosis with acceptable simplicity to check its functionality during operation. An *in situ* self-diagnostic technique for a dissolved oxygen microsensor is proposed in an effort to devise an intelligent microsensor system with an integrated electrochemical actuation electrode. With a built-in platinum microelectrode that surrounds the microsensor, two kinds of microenvironments, called the oxygen-saturated or oxygen-depleted phases, can be created by water electrolysis depending on the polarity. The functionality of the microsensor can be checked during these microenvironment phases. The polarographic oxygen microsensor is fabricated on a flexible polyimide substrate (Kapton®) and the feasibility of the proposed concept is demonstrated in a physiological solution. The sensor responds properly during the oxygen-generating and oxygen-depleting phases. The use of these microenvironments for *in situ* self-calibration is discussed to achieve functional integration as well as structural integration of the microsensor system.

Keywords – self-diagnosis, self-calibration, electrolysis, polyimide, intelligent microsensor.

I. INTRODUCTION

An intelligent microsensor system requires not only structural integration but also functional integration. In a biochemical microsensor system, special functionalities can be provided by the use of electrochemical "actuators" integrated with the sensor. Several electrochemical microactuators utilizing redox reactions of chemical species have been reported in combination with microsensors. A microscale pH titration system was first implemented by integrating a titration microelectrode with pH-ISFET (ion-sensitive field-effect transistor) [1]. Based on this concept, a long-term measurement of dissolved carbon dioxide was performed without the need for regular recalibration [2]. A similar structure has been used to demonstrate a potentiometric dissolved oxygen sensor based on pH sensing [3], which was later adopted in simultaneous measurement of cellular respiration and acidification with a single sensor [4]. With built-in iridium oxide actuators on top of the gate region of FET (field-effect transistor), novel potentiometric determinations of dissolved oxygen [5] and hydrogen peroxide [6] were accomplished. Microfludic systems including electrochemical actuators and sensors were reported to detect flow direction and to estimate flow velocity [7, 8]. Novel biosensors with built-in electrochemical actuation systems include a pH-static enzyme sensor to suppress the dependency of sensor response on sample solution pH [9] and a high-sensitivity potentiometric glucose sensor with the aid of an amperometric actuation system [10].

An ideal biosensor for long-term continuous monitoring should meet the following requirements: simple structure, immunity to motion artifacts, sufficient sensitivity for reliable measurements, robustness and stability over long periods of time, minimum inflammatory reaction with surrounding tissues during chronic implantation, and dependable diagnosis and/or calibration methods to check its functionality and accuracy. Numerous types of sensors for dissolved oxygen monitoring have been developed over the past decades (for a review, see references [11, 12]), and only limited successes have been achieved in spite of intensive efforts to meet these requirements. Apart from such long-term stability or biocompatibility, it should be emphasized that development of a novel *in situ* diagnosis technique without any externally coupled apparatus is one obstacle to the realization of an unattended intelligent microsensor system.

Consequently, we present a novel self-diagnosis concept for a dissolved oxygen microsensor by using an integrated electrochemical microactuator toward built-in intelligence of the microsensor system.

II. *IN SITU* SELF-DIAGNOSIS CONCEPT WITH ELECTROCHEMCIAL MICROACTUATOR

The principle of the novel diagnosis method proposed herein is based on water electrolysis at noble metal electrodes as shown in Figure 1. Oxygen or hydrogen can be generated by the electrolysis of water in a controlled manner by applying voltage or current through a generating electrode (GE) and counter-generating electrode (GE') [13]. Reactions occurring at the anode and cathode are as follows:

$$2H_2O \rightarrow 4H^+ + 4e^- + O_2 \quad \text{(at anode)} \qquad (1)$$

$$4H_2O + 4e^- \rightarrow 4OH^- + 2H_2 \text{ (at cathode)} \qquad (2)$$

Accumulation of these dissolved gas molecules at the generating electrode, in turn, rapidly establishes a microenvironment of oxygen saturation or hydrogen saturation. The accumulation and saturation of hydrogen molecules takes place after the depletion of oxygen. An oxygen microsensor in close proximity to the surrounded generating electrode can be confined in a controlled microenvironment. A two-point self-diagnostic procedure for the oxygen sensor can then be performed, with the high point diagnosis being established in an oxygen-saturated phase, and the low point diagnosis in an oxygen-depleted phase, respectively. These transient perturbations of the microenvironment are expected to equilibrate rapidly with the surrounding solution medium.

III. METHODS

1. Device design

We designed and fabricated polarographic micro-oxygen sensors on flexible polyimide substrates (Kapton®). The basic electrochemical three electrode cell configuration was adopted to avoid the ohmic voltage drop through the electrolyte between the anode and cathode. All electrodes were designed to be

geometrically symmetric to assure diffusional mass transport of electrochemical species in all radial directions. The noise at an electrode-electrolyte interface can be modeled by two sources [14] - 1/f noise and white noise. The 1/f noise is inversely proportional to the electrode area. A lower form factor for the electrode (the circumference to surface area ratio) results in a lower white noise level, which implies that the noise generated by a circular type electrode is lower than any other type of electrodes. Therefore we used a circular working electrode (WE). The conventional Clark oxygen sensor contains a reference electrode (RE) and a working electrode located in the same compartment filled with an internal electrolyte gel which is encapsulated by a hydrophobic, electrically non-conducting membrane. To circumvent the technical difficulties of fabricating the reliable double-layered membrane (electrolyte gel/hydrophobic membrane) [15, 16], we did not use any membrane in this study.

Figure 2 shows the layout and cross section of the concentric type electrode configuration. The middle electrode serves as the working electrode at which dissolved oxygen molecules are cathodically reduced. The generating electrode is wrapped around the working electrode; this configuration will establish oxygen-saturated or oxygen-depleted microenvironments during self-diagnosis phases. Proceeding from inside to outside, the next concentric circle can be used as the reference electrode. The outermost electrode in Figure 2 is the counter electrode (CE) of this three-electrode cell. It is placed at a distance from the working electrode to minimize electrochemical interference of byproducts generated at the counter electrode. The counter-generating electrode, not shown, is located even more remotely from the working electrode for this same reason.

2. Microfabrication

All of the prototype sensors were fabricated in the facilities of the Biomedical Microsensors Laboratory (BMMSL) at North Carolina State University [17]. All electrodes were platinum as shown in Figure 2 (b). Conventional platinum lift-off processes are difficult to execute on Kapton® substrates when organic solvent-based photoresist chemistries are required. This is because the long immersion in the solvents required for lift-off tends to degrade the adhesion of the metal to the Kapton® substrate. On the

other hand, wet chemical etching of platinum in heated aqua regia, while common on glassy substrates, was unsuccessful on Kapton® substrates for undetermined reasons. Instead, the substrates were first metallized with chromium and gold, but these layers were left unpatterned until after the deposition and lift-off of the platinum electrodes. This sequence has the advantage that the chromium and gold layer protects the Kapton® substrate from contact with the solvents during titanium and platinum lift-off.

Flexible polyimide substrates (Kapton®, Du Pont, type VN, 75 μm in thickness), were cleaned in successive rinses of acetone, methanol, and deionized water, and then dehydrated at 120 °C. A thin film of chromium as an adhesion layer, followed by a 0.2 μm film of gold was deposited on the substrate by DC magnetron sputtering. Positive photoresist (Shipley 1813) was spin-coated, selectively exposed through the photomasks with broad band UV light, and developed to pattern the electrode features. After deposition by DC magnetron sputtering of a thin titanium film and a 0.08 μm platinum film, the whole substrate was agitated in acetone to lift-off the photoresist layer along with unwanted titanium and platinum. Positive photoresist (Shipley 1813) was spin-coated again to protect the platinum layer during wet etching of the uncovered gold and chromium layers. After removal of the photoresist with solvents (Shipley 1165), the substrate was cleaned with organic solvents and dehydrated in preparation for the application of the polyimide dielectric layer. Photosensitive polyimide (HD Microsystems, Pyralin PI-2723) was spin-coated to a nominal thickness of 2.0 μm and exposed in the same manner as the photoresist. Subseqent development and thermal curing of the polyimide defined the platinum electrodes.

The use of a polyimide (Kapton®) substrate, which can be implemented as a flexible planar microsensor array, provides unique advantages for this specific application especially in terms of immunity to motion artifacts. Metal patterning to 10 μm line width was achieved. Smaller line widths are possible, but are more difficult due to thermal expansion of the Kapton® substrate during the microfabrication process and surface roughness of the substrate. The electrochemical properties of each sensor from same wafer were showed some nonuniformity. In the future, we envision an optimized microfabrication process that includes more precise photolithography with higher resolution and the

supporting the flexible substrate during processing with a rigid wafer to minimize thermal instability and substrate roughness.

3. Measurements

The fabricated Kapton®-based oxygen microsensor was connected to the test instruments via a zero-insertion force (ZIF) connector and cable as shown in Figure 3. A commercial miniature reference electrode (Harvard Apparatus, AH69-0024) was used in this study in place of the on-chip reference electrode to avoid possible instability of thin film Ag/AgCl electrode caused by electrochemical crosstalk with hydrogen peroxide which is a byproduct of the reaction [18]. The sensor was placed in a measuring vessel and the solution was saturated with different oxygen/nitrogen gas ratios at room temperature. Oxygen tension in the bulk solution was monitored with a commercial oxygen meter (Instech, SYS203). All measurements were done in a stationary solution to prevent any solution convectional effects.

A custom set of electrochemical instrumentation has been employed. A potentiostat (Gamry Instruments, FAS1) and a galvanostat (Gamry Instruments, 750) were used to bias the 3-electrode oxygen microsensor and to operate the generating electrodes, respectively. These two modules were plugged into one control PC and operated in a floating-ground mode to prevent electrical interference between the two modules. The cathodic potential for oxygen reduction (-0.7 V vs. Ag/AgCl) was chosen from the plateau region in a traditional voltammogram. To control the microenvironment near the working electrode of the oxygen microsensor, constant currents were forced between the pair of generating and counter-generating electrodes. Figure 4 shows a schematic of the measurement system.

A script was written to perform two different procedures for the establishment of microenvironments. First, the operation of the system was divided into a generation phase and followed by a measurement phase (mode (a) in Figure 4). After a predefined gas-generating phase, the oxygen sensor was triggered by the potentiostat, which provides a potential step to the working electrode for oxygen reduction and then makes chronoamperometric measurements of the sensor's response. Any change in the microenvironment during the generating phase will affect transient response of the sensor.

This two-phase process helps eliminate any possible electrostatic coupling between the three-electrode oxygen microsensor and the generating electrode source. The second calibrating procedure involved a simultaneous gas-generating phase during sensor operation (mode (b) in Figure 4). By this procedure, monitoring of any changes in the microenvironment during the preceding generating phase is possible by comparing real-time measurements with the sensor's baseline response, which reflects the background oxygen content. After each measurement, the solution was equilibrated to a defined baseline value by bubbling with a fixed ratio of oxygen and nitrogen gases and magnetically stirring.

IV. RESULTS AND DISCUSSION

1. Characterization of the working and generating electrodes

Every new device was pre-polarized for about 30 minutes at the cathodic potential for oxygen reduction (-0.7 V vs. Ag/AgCl) before the actual measurements to obtain stabilized values. Figure 5 shows typical chronoamperometric responses of the oxygen microsensor with a platinum working electrode in various bulk oxygen contents. Typical chronoamperometric responses are first observed at the onset of potential pulses to the working electrode. Afterwards the current reaches a steady-state value, which is called an oxygen limiting current. According to the limiting current theory, the relationship between limiting current magnitude and oxygen content is linear over the entire concentration range. The pH change during the oxygen reduction at the working electrode is considered to attribute to the nonlinearity of current magnitude versus oxygen content in Figure 5. It is known that the stoichiometric coefficient of oxygen reduction, between 2.0 and 4.0, depends on bulk solution pH [19]. Oxygen reduction occurs predominantly in a single 4-electron step at low bulk solution pH:

$$O_2 + 2H_2O + 4e^- \rightarrow 4OH^- \qquad (3)$$

And an increase in bulk pH increases the proportion of two-electron step:

$$O_2 + 2H_2O + 2e^- \rightarrow H_2O_2 + 2OH^-, \quad H_2O_2 + 2e^- \rightarrow 2OH^- \qquad (4)$$

As the oxygen concentration increases, the decrease in pH change at the surface of the working electrode (i.e. the accumulation of OH^- ions) becomes more significant to reduce the stoichiometric coefficient. Other factors that influence this coefficient, such as electrode material, reduction potential, surface aging and pretreatment, remained the same in this study.

Figure 6 shows a cyclic voltammogram of a platinum generating electrode in an air-saturated phosphate buffer solution (10 mM, pH 7.4). Oxygen and hydrogen peaks can be seen at the right and left edges of the water electrolysis window, respectively. The minimum generating current was chosen to be 49 nA (0.5 mA/cm^2) for oxygen generation and – 147 nA (– 1.5 mA/cm^2) for oxygen depletion, respectively, to ensure high current efficiency for water electrolysis during the establishment of the microenvironments. Selecting a generating electrode material with a narrower water electrolysis window will have benefits for this application by maximizing the current efficiency for electrolyzing water and minimizing the power consumption.

2. Transient response preceded by a separate generating phase

Constant generating currents were driven through the generating (anode) and counter-generating electrodes (cathode) for up to 90 seconds to establish a stable microenvironment around the working electrode. Transient chronoamperometric responses in an air-saturated solution were recorded immediately following the generating phase as described in Figure 4 (a). As the duration of generating current pulses increases, the magnitudes of initial transient response increase as shown in Figure 7 (a). This means that a steady-state oxygen-rich environment has been established in the vicinity of the sensor as expected since a larger number of oxygen molecules were generated by the longer current durations. Convergence of all curves to bulk oxygen value (response to the air-saturated solution) means that the oxygen-rich environment is being equilibrated with the surrounding medium. With a generating current density of 5 mA/cm^2 the effect of generating current durations of longer than 30 seconds was about the same, suggesting that the degree of oxygen accumulation around the sensor in the generating phase reaches steady-state after about 30 seconds. Shortly after the completion of these measurements in the air-

saturated environment, the solution was saturated with 100 % oxygen to compare the sensor response. Note that the initial peaks after the generation phase in the air-saturated solution approach that obtained in the oxygen-saturated solution. A similar procedure was then applied to observe the transient response of the sensor after an oxygen-depleting phase provided by reversing the current direction through the generating electrode. Figure 7 (b) shows typical responses of another sensor from the same wafer. The response after the depleting phase shows a reduced initial height followed by a recovery to the bulk response.

The main factors governing this microenvironment are the diffusion coefficient and mobility of the generated molecules (dissolved gases, hydrogen and hydroxyl ions) in the sample solution. These electrochemical parameters will be affected by the solution composition. Also the electrode kinetics (oxygen reduction at the working electrode, redox processes for oxygen/hydrogen generation, and hydrogen/hydroxyl ion production at the generating electrode) may be affected by electrochemical interference of species in the sample solution. Sensor geometry, especially the spacing between working and generating electrodes, will be the predominant parameter to determine the optimum conditions to control the microenvironment, which is a critical element in the performance of the *in situ* self-diagnosis sensor. A small electrode area and close spacing between the electrodes is required to reduce the overall sensor size and to minimize oxygen consumption by the sensor itself. The sensor's geometric structure should be optimized to minimize the duration and magnitude of the generating signal.

3. Quasi steady-state response during a simultaneous generating phase

The generating phase was performed during the normal operation of the sensor for the mode of operation described in Figure 4 (b). Once the limiting current condition at a given bulk oxygen content had been achieved after application of the oxygen reduction potential to the sensor, the generating current were applied to the generating electrode for 90 seconds. The limiting current level (the baseline during the response) reflects the bulk oxygen content around the sensor. Various time responses during the generating phase are shown in Figure 8 (a). Simultaneous operation of the potentiostatic instrument (for

biasing the oxygen microsensor) and the galvanostatic instrument (for driving the generating current) produced a quasi steady-state response during the generating phase. For comparison the response to oxygen-saturation was recorded shortly after the completion of these measurements in the air-saturated case in the same solution. It can be seen that the responses during each generating phase approaches the limiting current levels of the oxygen-saturated solution and then gradually returns to the original level of bulk oxygen content. As the generating current density increases the corresponding response increases, which agrees with the result shown in Figure 7 (a). With the current density higher than 16 mA/cm^2, tarnish on the generating electrode surface and damage to the polyimide encapsulation were observed occasionally in some of the devices.

At a given temperature, the limiting current magnitude in the oxygen-saturated solution (100% oxygen-saturation) is limited to 4.76 times of that in the air-saturated solution (21% oxygen-saturation) at 1 atm. During the generating phase with higher generating current densities, however, responses exceeding this limit were observed. The most plausible explanation for this is the supersaturation of the electrochemically generated oxygen in the microenvironment covering the working electrode [20]. The concentration of the electrochemically generated oxygen near the oxygen-evolving anode surface can exceed the standard oxygen solubility in water at 1 atm without the formation of gas bubbles. The pH change in the microenvironments due to water electrolysis is also expected to have contributed to this exaggerated response. The generation of dissolved oxygen and hydrogen is accompanied by a pH shift at the electrode surface as shown in equations (1) and (2), which means the microenvironment will undergo pH changes during the generating phases. Subsequently, the oxygen catalytic activity of the platinum working electrode should be enhanced by the lower pH induced in the microenvironment according to equation (3) during this phase.

To observe the overall influence of pH and supersaturation, the generating phase was performed in an oxygen-saturated solution. The lower curve in Figure 8 (b) is a plot of the percent changes of response during the oxygen-generating phase with respect to the baseline at the oxygen-saturated solution. At the highest current density the response was almost doubled from the baseline (response to the oxygen-

saturated solution), suggesting that either the stoichiometric coefficient was increased or supersaturation was established, or both. To further investigate the influence of the pH changes during the oxygen-generating phase, measurements were performed in solutions with different pH buffering capacities. The response magnitudes in a 1 mM buffer solution were most pronounced, which implies that in stronger buffer solutions the pH changes were suppressed to minimize the perturbation of the stoichiometric coefficient of oxygen reduction. At the highest current density, the responses during the generating phase were similar with the oxygen-saturation value (theoretically 476%) in 10 mM and 100 mM buffer solution. This suggests that an *in situ* high-point calibration (100% oxygen) can be accomplished by establishing an oxygen-saturated microenvironment with a refined device structure and generating signal.

Other factors may have contributed to the exaggerated responses; first, a considerable concentration-driven convection by the oxygen molecules diffusing from the generating electrode could enhance the mass transport of oxygen in the stagnant solution, thereby increasing the limiting current value of the oxygen-saturated solution. A second factor may be "feedback" of electrochemically generated oxygen generated from hydrogen peroxide [18], a byproduct of oxygen reduction at the working electrode as in equation (4). Hydrogen peroxide is being oxidized to oxygen at the anodic generating electrode and contributes to the oxygen-rich microenvironment.

$$H_2O_2 \rightarrow 2H^+ + O_2 + 2e^- \qquad (5)$$

Thirdly, the possibility of temperature elevation around the microsensor due to high current densities. The generation of gas bubble has not been monitored during this study. Further analysis of these factors is necessary to adapt the proposed system for practical applications.

The effect of stirring on the microenvironment was also investigated. As expected, the magnitude of response diminished with energetic stirring of the solution as in Figure 8 (c). The response of the same sensor without solution stirring is given for comparison. Note the increased baseline produced by stirring. This result allows us to ascertain that the contribution of electrical interference to the response by the potentiostat operating the oxygen microsensor and the galvanostat operating the generating electrode pair is negligible.

Figure 9 (a) shows the quasi-steady state responses during the oxygen-depleting phase. Analogous to the generating phase, the sensor responses during depleting phases approach the limiting current levels at nitrogen-saturation, followed by a return to the original level of bulk oxygen content. As the current density increases the corresponding response decreases, which is consistent with Figure 7 (b). It should be noted from Figure 9 (b) that the responses with the current density higher than 5 mA/cm^2 remains around 30 % of the bulk response without significant decrease beyond this level. This implies that the oxygen depletion has not been completely accomplished with the given electrode geometry over the entire current density range. The higher pH in the microenvironment during the depleting phase is assumed to further decrease the sensor response due to the reduction of catalytic activity of the working electrode to reduce oxygen. Improvements in sensor structure are expected to achieve a low-point *in situ* calibration during the sensor operation.

Incorporation of a Clark type microsensor structure should minimize the pH effects and possible electrical interference caused by the galvanostat. By encapsulating a 3-electrode oxygen sensor within a double-layer gas permeable membrane, consisting of an outer hydrophobic and an inner hydrophilic layer, the oxygen sensor itself can be fully isolated from the surrounding generating electrode. However, microfabrication of a reliable and repeatable double-layered polymeric structure is challenging. In addition, lower oxygen permeability with the double-layer membrane will cause longer response time and will require a higher amplitude and longer duration of the generating signal.

VI. CONCLUSION

The concept of an *in situ* self-diagnostic technique for a dissolved oxygen microsensor is proposed in an effort to devise an intelligent microsensor system with an integrated electrochemical actuation electrode. The feasibility of the proposed concept is demonstrated in a physiological solution. The sensor responds properly during both the oxygen-generating and oxygen-depleting phases. The integrated electrochemical actuator is a useful tool for achieving built-in intelligence of the dissolved

oxygen microsensor. The results suggest that the use of these microenvironments for *in situ* self-diagnosis and *in situ* self-calibration can be expected with carefully refined microstructures and generating signals. This intelligent capability of oxygen microsensors is needed to improve their reliability during their *in situ*, and potentially *in vivo*, operation.

ACKNOWLEDGEMENTS

This research was supported partly by a grant from the NASA Office of Biological and Physical Research (01-OBPR-01), and by Sicel Technologies, Inc., Research Triangle Park, North Carolina.

REFERENCES

1. B. H. van der Schoot and P. Bergveld, "An ISFET-based microlitre titrator: integration of a chemical sensor-actuator system," Sensors and Actuators, Vol. 8, pp. 11-22, 1985.
2. B. H. van der Schoot and P. Bergveld, "Coulometric sensors: the application of a sensor-actuator system for long-term stability in chemical sensing," Sensors and Actuators, Vol. 13, pp. 251-262, 1988.
3. B. K. Sohn and C. S. Kim, "A new pH-ISFET based dissolved oxygen sensor by employing electrolysis of oxygen," Sensors and Actuators B-Chemical, Vol. 34, pp. 435-440, 1996.
4. M. Lehmann, W. Baumann, M. Brischwein, H. J. Gahle, I. Freund, R. Ehret, S. Drechsler, H. Palzer, M. Kleintges, U. Sieben, B. Wolf, "Simultaneous measurement of cellular respiration and acidification with a single CMOS ISFET," Biosensors and Bioelectronics, Vol. 16, No. 3, pp. 195-203, 2001.
5. J. Hendrikse, W. Olthuis and P. Bergveld, "The ^{E}MOSFET as an oxygen sensor: constant current Potentiometry," Sensors and Actuators B-Chemical, Vol. 59, pp. 35-41, 1999.

6. T. W. A. Dam, W. Olthuis and P. Bergveld, "Electroactive gate materials for a hydrogen peroxide sensitive ^{E}MOSFET," IEEE Sensors Journal, Vol. 2, pp. 26-33, 2002.
7. J. Wu and W. Sansen, "Electrochemical time of flight flow sensor," Sensors and Actuators B-Chemical, Vol. 97-98, pp. 68-74, 2002.
8. A. Poghossian, J. W. Schultze and M. J. Schoning, "Multi-parameter detection of (bio-)chemical and physical quantities using an identical transducer principle, Sensors and Actuators B-Chemical, Vol. 91, No. 1-3, pp. 83-91, 2003.
9. B. H. van der Schoot, H. Voorthuyzen and P. Bergveld, "pH-static enzyme sensor. Design of the pH control system," Sensors and Actuators B-Chemical, Vol. 1, No. 1-6, pp. 546-549, 1990.
10. H. I. Seo, C. S. Kim, B. K. Sohn, T. Yeow, M. T. Son and M. Haskard, "ISFET glucose sensor based on a new principle using the electrolysis of hydrogen peroxide," Sensors and Actuators B-Chemical, Vol. 40, pp. 1-5, 1997.
11. F. Kreuzer, H. Kimmich, M. Brezina and J. Heyrovsky, "Polarographic determination of oxygen in biological materials," in J. Koryta (ed.), *Medical and biological applications of electrochemical devices*. John Wiley & Son, 1980, pp. 173-261.
12. I. Fatt, *The polarographic oxygen sensor: its theory of operation and its application in biology, medicine, and technology,* CRC Press, 1976.
13. C. S. Kim, J. O. Fiering, C. W. Scarantino and H. T. Nagle, "A novel in situ self-calibration method for an oxygen microsensor," World Congress on Medical Physics and Biomedical Engineering, Abstract No. WE-Ba205-02 (CD-ROM), Chicago, USA, 2000.
14. M. Lambrechts and W. Sansen, *Biosensors: microelectrochemical devices,* IOP Publishing, 1992, pp. 206-208.
15. G. Jobst, G. Urban, A. Jachimowicz, F. Kohl, O. Tilado, I. Letternbichler and G. Nauer, "Thin-film Clark-type oxygen sensor based on novel polymer membrane systems for in vivo and biosensor applications," Biosensors and Bioelectronics, Vol. 8, pp. 123-128, 1993.

16. Ph. Arquint, A. van den Berg, B. H. van der Schoot, N. F. de Rooij, H. Buhler, W. E. Morf and L. F. J. Durselen, "Integrated blood-gas sensor for pO_2, pCO_2 and pH," Sensors and Actuators B-Chemical, Vol. 13-14, pp. 340-344, 1993.

17. R. P. Buck, V. V. Cosofret, E. Lindner, S. Ufer, M. B. Madaras, T. A. Johnson, R. B. Ash and M. R. Neuman, "Microfabrication technology of flexible membrane-based sensors for in-vivo applications," Electroanalysis, Vol. 7, pp. 846-851, 1995.

18. C. S. Cha, M. J. Shao and C. C. Liu, "Problems associated with the miniaturization of a voltammetric oxygen sensor: chemical crosstalk among electrodes," Sensors and Actuators B-Chemical, Vol. 2, pp. 239-242, 1990.

19. V. Linek, V. Vacek, J. Sinkule and P. Benes, *Measurement of Oxygen by Membrane-covered Probes*, Ellis Horwood, 1988. pp. 17-24.

20. S. Bohm, W. Olthius and P. Bergveld, "An integrated micromachined electrochemical pump and dosing system," Journal of Biomedical Microdevices, Vol. 1, No. 2, pp. 121-130, 1999.

FIGURE CAPTIONS

Figure 1. Concept for a novel oxygen sensor with *in situ* self-diagnosis capability. The microenvironment is generated by a generating electrode (GE) which surrounds the microsensor. Oxygen-saturated or oxygen-depleted phases can be established by water electrolysis depending on the polarity.

Figure 2. Concentric 3-electrode oxygen sensor with total diameter of 200 micron meter, (a) Layout of exposed electrodes (not to scale), (b) cross-sectional view after fabrication on a flexible Kapton® substrate (1. substrate cleaning, 2. Au/Cr deposition, 3. Pt/Ti deposition, 4. Pt/Ti lift-off, 5. Au/Cr etching, 6. polyimide patterning).

Figure 3. Photograph of a probe assembly. An oxygen microsensor fabricated on flexible Kapton® substrate (upper right part) is connected to a ribbon cable via a zero-insertion force (ZIF) connector (lower part).

Figure 4. Measurement scheme. A potentiostat and a galvanostat are employed for biasing the 3-electrode oxygen microsensor and for generating microenvironments, respectively, (a) Sequential generating mode for transient response, (b) Simultaneous generating mode for quasi steady-state response.

Figure 5. Time responses (chronoamperometry) of the oxygen reduction current at a Pt working electrode responding to potential step (-0.7 V vs. Ag/AgCl) in phosphate buffer solution (pH 7.4, 10 mM) with various oxygen contents.

Figure 6. Voltammogram of a Pt generating electrode in air-saturated phosphate buffer solution (pH 7.4, 10 mM, scan rate: 50 mV/sec).

Figure 7. Typical transient responses after an initial generating phase in air-saturated phosphate buffer solution (pH 7.4, 10 mM), (a) effect of oxygen-generating phase with current pulses (5 mA/cm^2) on the generating electrode with various durations, with a sensor response to oxygen-saturated solution for comparison, (b) effect of oxygen-depleting phase with current pulses (same pulse in the opposite polarity) on the generating electrode with various durations, with a sensor response to nitrogen-saturated solution for comparison.

Figure 8. Typical quasi steady-state responses during the simultaneous oxygen-generating phase, (a) effect of the oxygen-generating phase with various current densities in air-saturated phosphate buffer solution (pH 7.4, 10 mM), with a sensor response to oxygen-saturated solution for comparison, (b) percent changes in the sensor responses (ratio of the steady-state value at t=90 with respect to the baseline at t=0) according to the generating current density in various pH buffering capacities, with those in an oxygen-saturated solution for comparison, (c) effect of vigorous solution stirring in air-saturated phosphate buffer solution (pH 7.4, 10 mM), with a sensor response to a stationary solution for comparison.

Figure 9. Typical quasi steady-state responses during the simultaneous oxygen-depleting phase in air-saturated phosphate buffer solution (pH 7.4, 10 mM), (a) effect of the oxygen-depleting phase with various current densities, with a sensor response to nitrogen-saturated solution for comparison, (b) percent changes in the sensor responses (ratio of the steady-state value at t=90 with respect to the baseline at t=0) according to the generating current density.

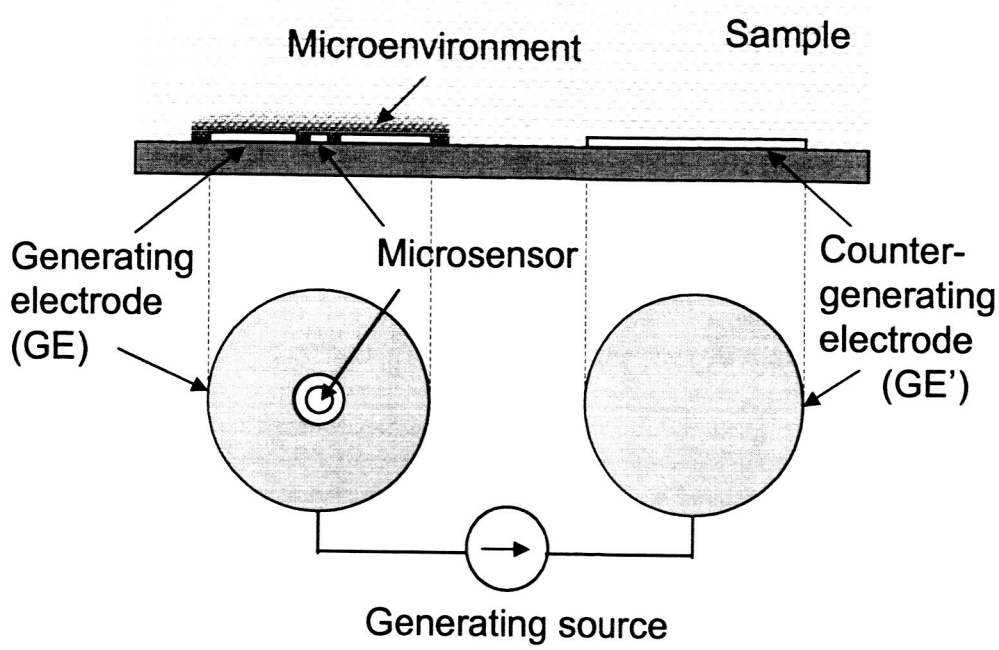

Figure 1.

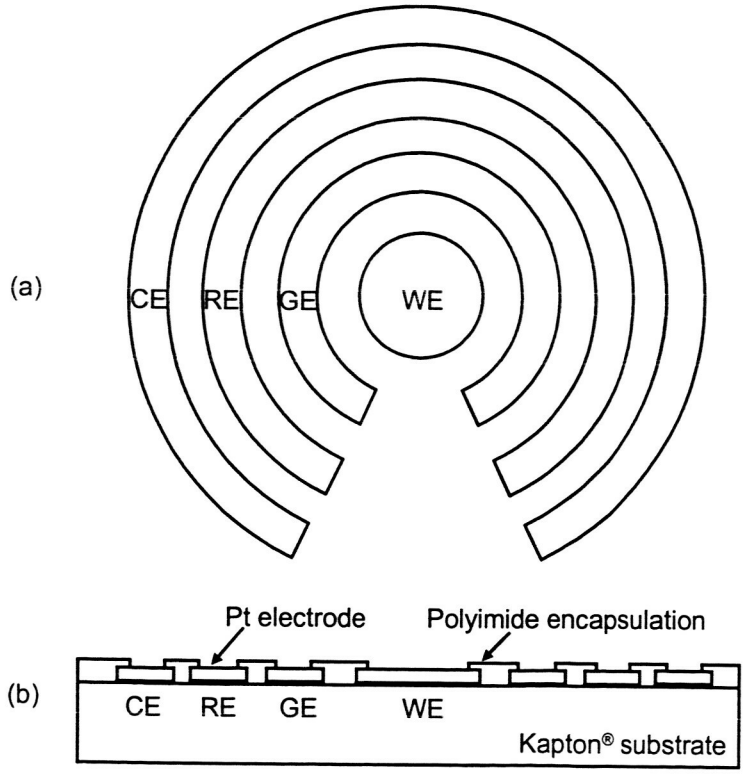

Figure 2.

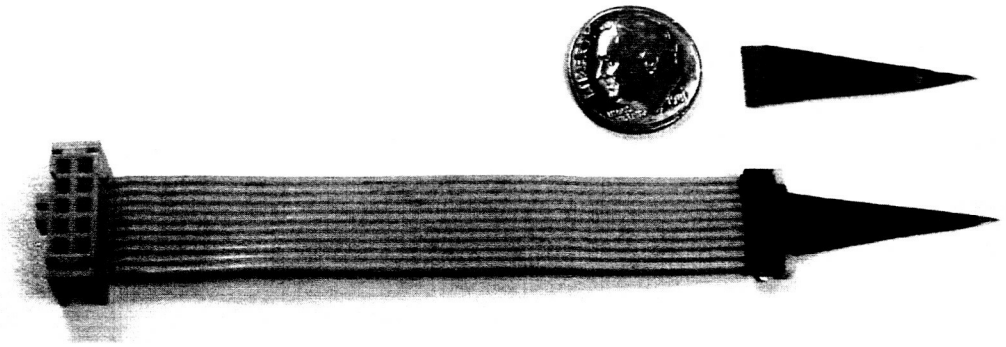

Figure 3.

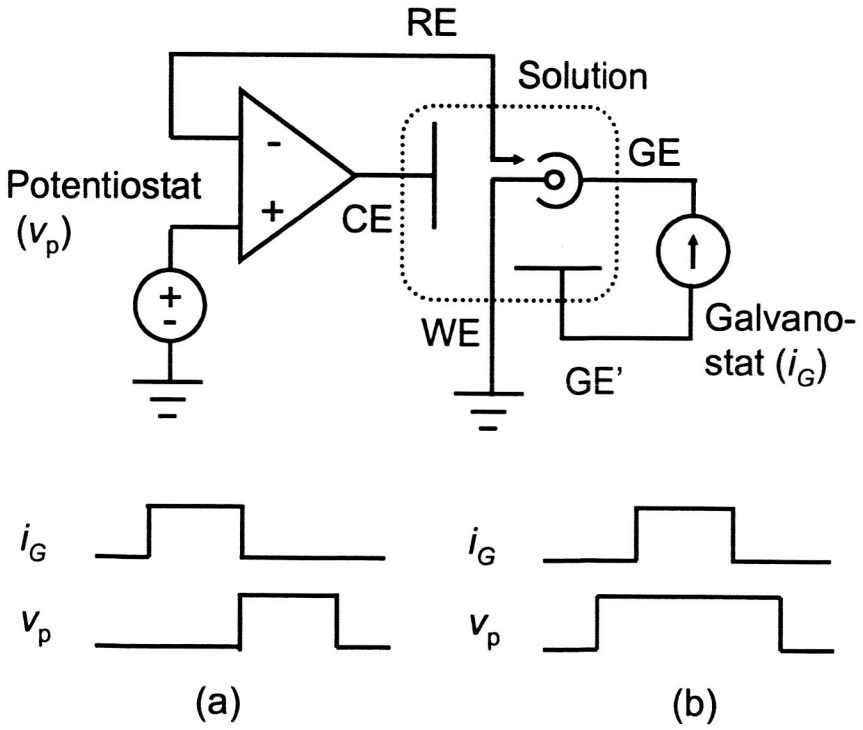

Figure 4.

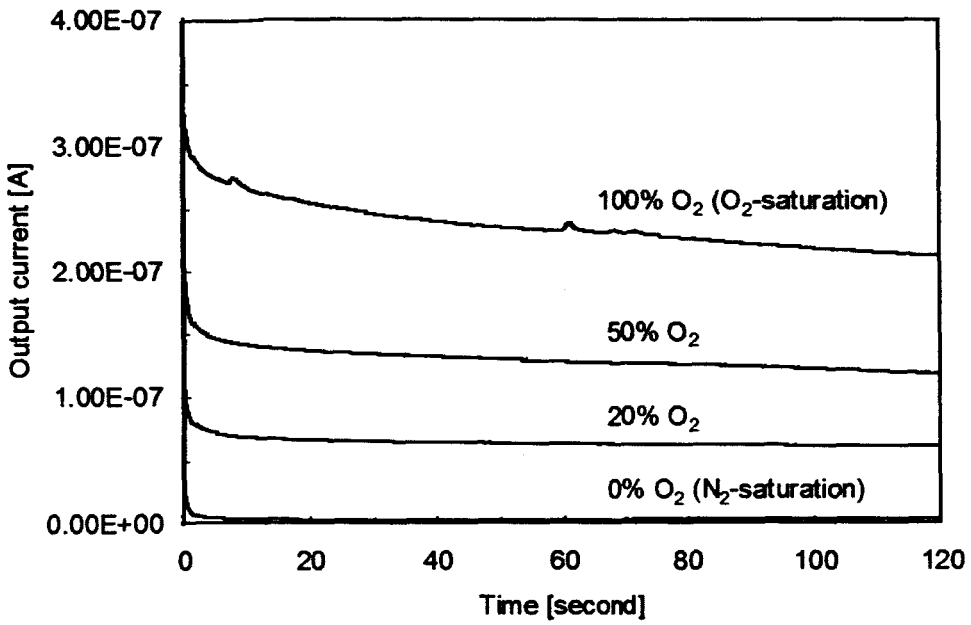

Figure 5.

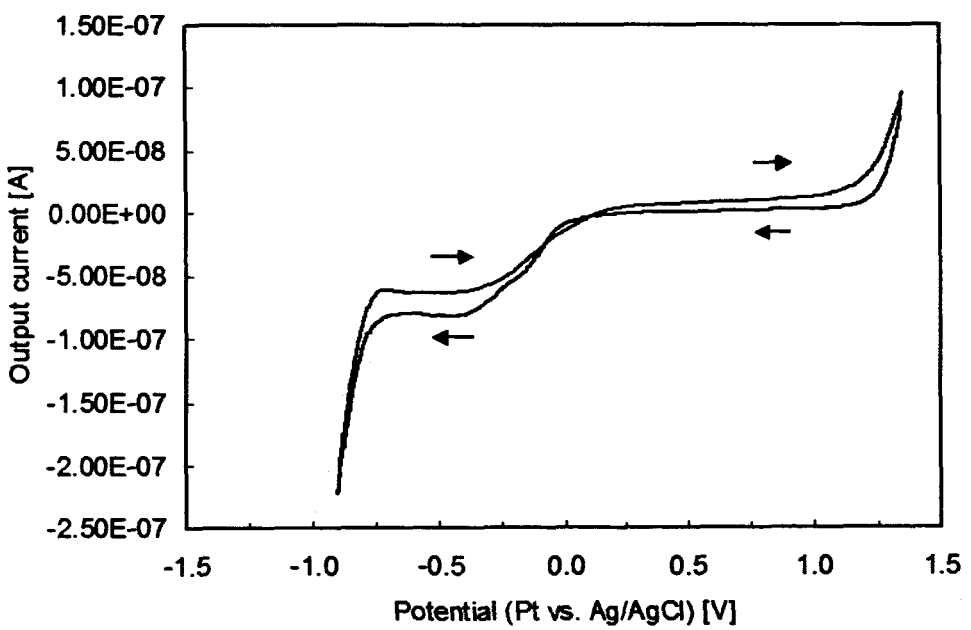

Figure 6.

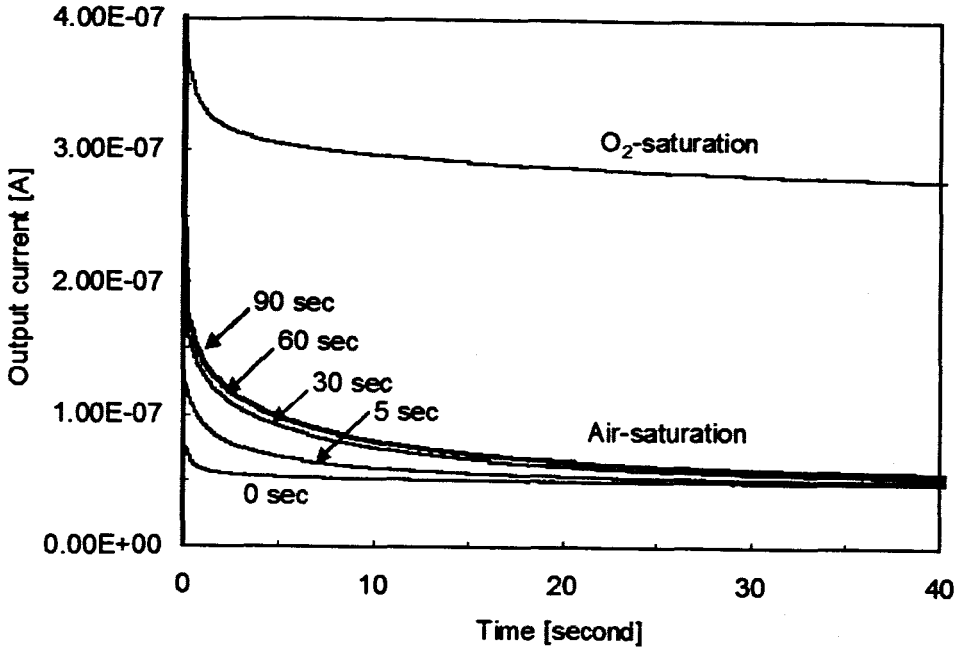

(a)

Figure 7 (a).

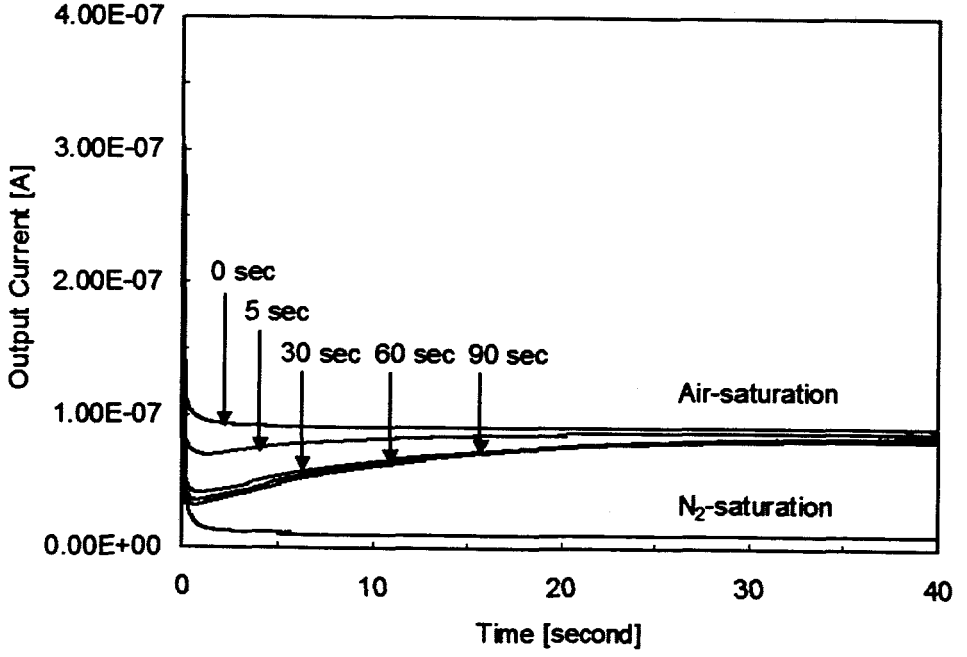

(b)

Figure 7 (b).

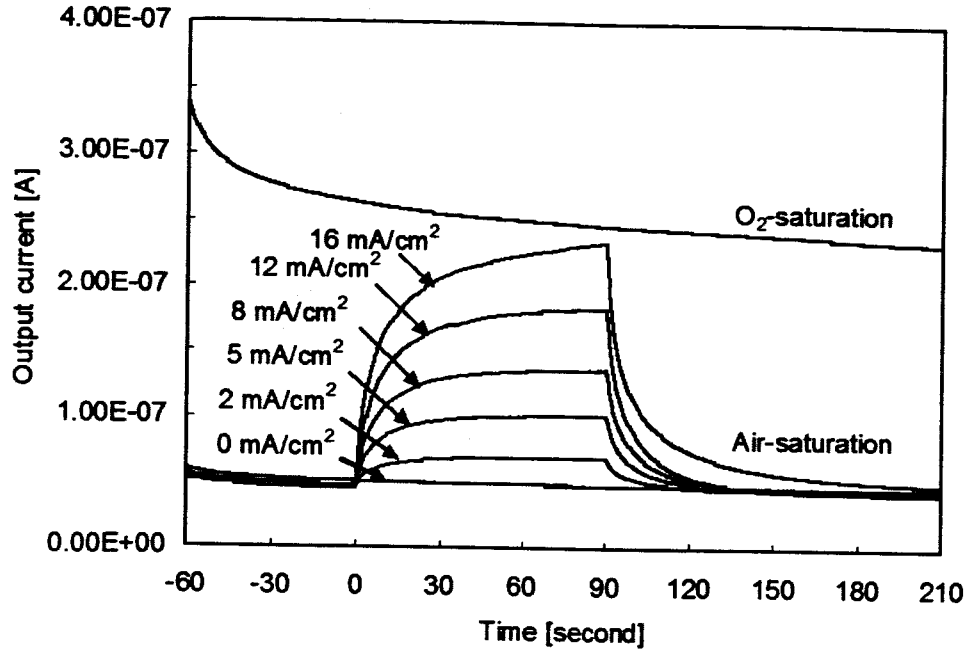

(a)

Figure 8 (a).

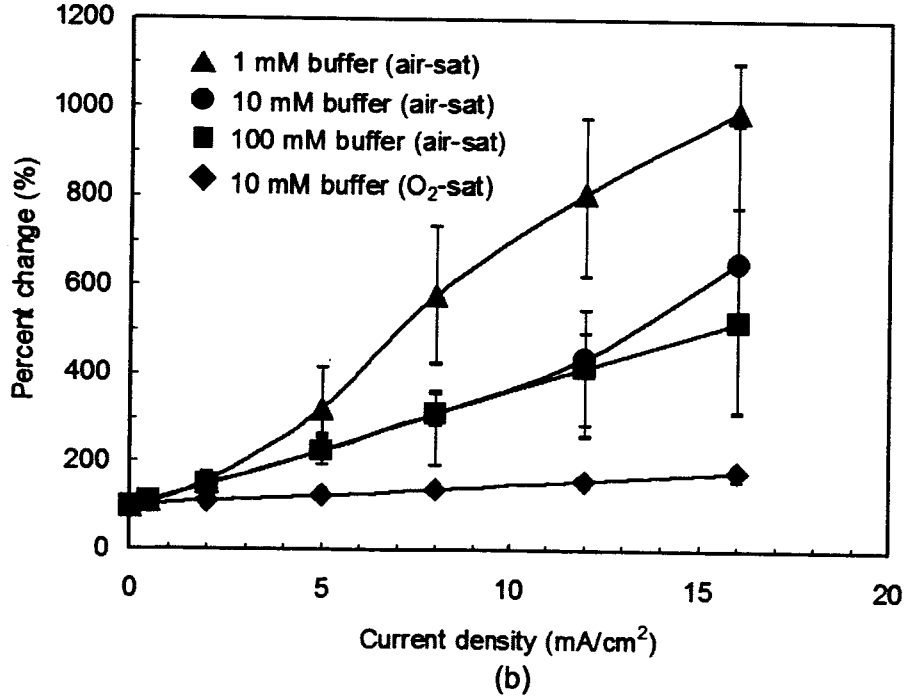

(b)

Figure 8 (b).

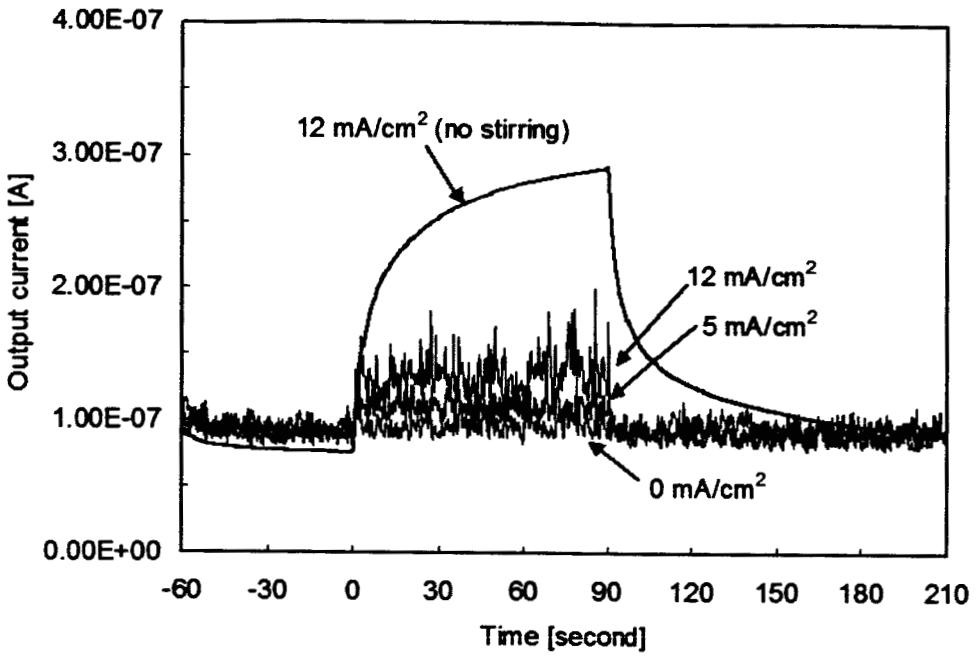
4.00E-07
3.00E-07
2.00E-07
1.00E-07
0.00E+00
Output current [A]
12 mA/cm2 (no stirring)
12 mA/cm2
5 mA/cm2
0 mA/cm2
-60
-30
0
30
60
90
120
150
180
210
Time [second]

(c)

Figure 8 (c).

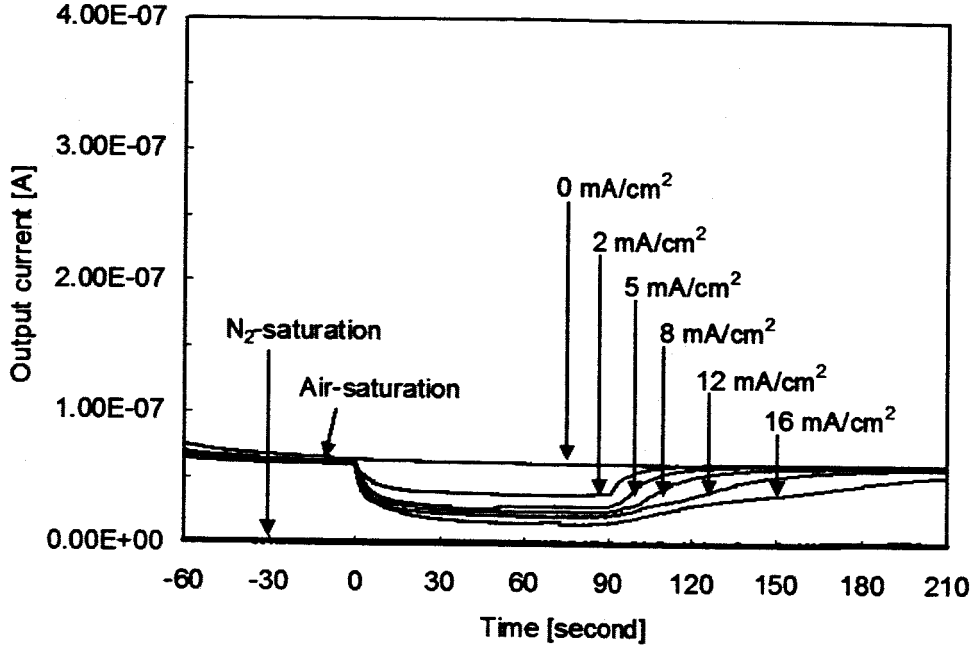

(a)

Figure 9 (a).

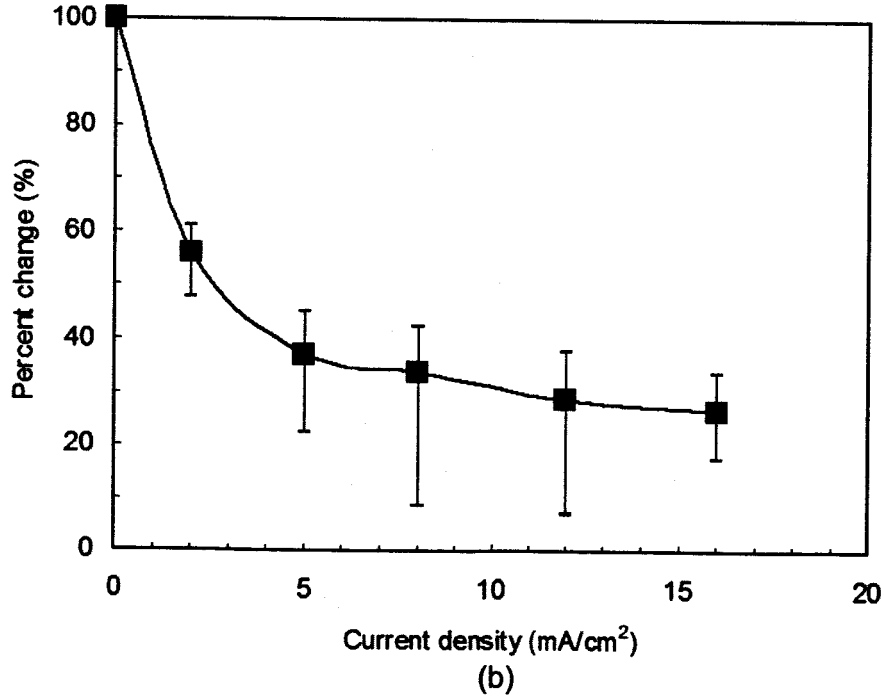

(b)

Figure 9 (b).